REPORT NO.
UCB/SEMM-88/18

STRUCTURAL ENGINEERING,
MECHANICS AND MATERIALS

4-NODE AXISYMMETRIC ELEMENT BASED UPON THE HELLINGER-REISSNER FUNCTIONAL

by

SHMUEL L. WEISSMAN

and

ROBERT L. TAYLOR

OCTOBER 1988

DEPARTMENT OF CIVIL ENGINEERING
UNIVERSITY OF CALIFORNIA
BERKELEY, CALIFORNIA

4-NODE AXISYMMETRIC ELEMENT BASED UPON THE HELLINGER-REISSNER FUNCTIONAL

Shmuel L. Weissman & Robert L. Taylor
Department of Civil Engineering, University of California, Berkeley

Abstract - The Hellinger-Reissner functional is used to formulate axisymmetric elements of the correct rank using seven and eight parameter stress fields. The resulting elements exhibit excellent performance in bending problems and at the nearly incompressible limit. The stress field is developed in conjunction with an orthogonal projection so that the resulting stiffness matrix requires only block diagonal inversion. Several numerical examples are given to demonstrate the performance of the suggested formulation.

0. Introduction

Solution of problems by the finite element method require that certain requirements be fulfilled by the formulation employed. Lax & Richtmyer [1956] proved that consistency and stability are necessary and sufficient requirements for a linear problem to converge. Isoparametric formulations are known to satisfy consistency and stability conditions provided sufficient order quadrature is used (Bicanic & Hinton [1979]). However, equally well known is the "locking" behavior of this type of formulation for the plane strain and axisymmetric linear isotropic elasticity models with high Poisson ratio (e.g., $\nu > 0.499$). Accordingly, it is evident that "good" element performance goes beyond the minimum requirements for convergence. It is commonly accepted that elements should have the following properties :

a) High accuracy over wide ranges of problem types and material properties.

b) Stable solutions for all type of boundary conditions.

c) Insensitive to element distortion and mesh configuration.

d) Perform independent of coordinate system or user input of data.

This paper considers the development of elements which satisfy the above conditions for the torsionless axisymmetric problem. The finite element formulation of the torsionless axisymmetric problem is almost identical with the plane strain formulation (Hughes [1987]). Indeed, both elements normally can be combined at a low overhead. As noted above, the isoparametric fully-integrated axisymmetric element locks at the nearly incompressible limit. Also, this element is overstiff when applied to bending problems (e.g., see pp. 221 of Hughes [1987]). The similarity of these formulations suggests that techniques used to overcome the problems in the plane strain case also can be applied to the axisymmetric case.

The simplest way to overcome the locking at the nearly incompressible limit is to use an under-integrated stiffness matrix. The stiffness matrix satisfies necessary accuracy (consistency) requirements, however, it does not meet stability requirements. To overcome this setback, Hughes [1977] applied the selective reduced integration (SRI) technique to develop element stiffness matrices through the assumed displacement method. The SRI scheme used under-integration on the volumetric strain terms and full-integration on the deviatoric terms. Malkus & Hughes [1978] showed that the SRI method falls within the concept of the mixed finite element method for plane strain and three-dimensional analysis. This analogy, however, breaks down in the axisymmetric case. Hughes [1987] suggested that a mixed formulation will lead to superior elements.

Hughes [1980] refined the SRI scheme into a general B-bar method for three-dimensional and axisymmetric elements. More recently, Simo, Taylor & Pister [1985] showed that it is possible to derive the B-bar method from the Hu-Washizu variational principle.

Belytschko and co-workers, (see e.g., Belytschko, Liu, Ong & Kennedy [1984] and Liu & Belytschko [1984]) took a different approach to overcome the problem of locking at the nearly

incompressible limit. Using a projection operator, Belytschko & Bachrach [1986] showed that the usual finite element approximation can be rewritten in a form that leads to decoupling of the stiffness matrix in the plane strain/stress cases. The decoupling of the stiffness matrix for the plane cases consists of an under-integrated stiffness matrix and a "stabilization" stiffness matrix. This decoupling leads to an efficient implementation as well as to a better understanding of element behavior in limit situations (such as the nearly incompressible limit). Bachrach & Belytschko [1986] applied this technique to the axisymmetric problem. The elements presented employ only seven independent interpolants in the stress and strain fields, thus obtaining the correct rank using a minimum number of independent interpolants. The best of the elements presented is called the optimal axisymmetric bending/incompressible (OABI). This element doesn't lock at the nearly incompressible limit and seems to yield good results in terms of the bending problem. This element, however, is not coordinate frame invariant.

Pian & Sumihara [1984] presented a plane strain element that has excellent characteristics at the nearly incompressible limit and also in bending applications. In addition, the element sensitivity to mesh distortions from a parallelogram shape appears to be the smallest of any 4-node element evaluated to date. Using the Hellinger-Reissner variational principle, Pian & Chen [1983] showed it is possible to obtain an axisymmetric element of the correct rank using seven independent interpolants in the stress field.

This paper presents 4-node axisymmetric elements that will perform well for all Poisson ratios and for the bending problem. The Hellinger-Reissner variational principle is used to derive the stiffness matrix. The stress field presented by Pian & Sumihara [1984] is modified to account for the differences between the axisymmetric and plane strain elements, i.e., only one physical, rigid body motion mode is present in the axisymmetric case whereas three modes are present, in the plane strain case. The projection operator, introduced by Belytschko, together with the modified stress field leads to an elegant formulation of the stiffness matrix.

Section 1 begins with a presentation of the equivalent form of the finite element approximation based on the projection operator. Also included are some basic quantities that are useful in deriving the stiffness matrix. The stiffness matrix based on the Hellinger-Reissner variational principle is formulated in section 2, and numerical results which demonstrate the performance of the different stress field approximations are presented in section 3.

1. Alternative Finite Element Approximation and Basic Quantities

This section presents an equivalent form to the usual finite element approximation. This form is based on the γ projection operator, first introduced by Flanagan & Belytschko [1981]. This equivalent form leads to a better understanding of the element topology. Also included are some basic quantities used to derive the element stiffness matrix.

Finite element approximation of a variable U over the element *area* Ω_e (i.e., $\Omega_e = dr\,dz$) is given by

$$U(\xi,\eta) = \sum_{I=1}^{4} N_I(\xi,\eta)\, U_I \tag{1.1}$$

where N_I is the shape function. For the 4-node element, the shape function is given by

$$N_I(\xi,\eta) = \frac{1}{4}(1+\xi_I\,\xi)(1+\eta_I\,\eta) \tag{1.2}$$

With ξ_I and η_I the natural coordinates for each node (see Fig. 1.1). Flanagan & Belytschko [1981] introduced the γ projection operator that allowed replacing (1.1) by

$$U(\xi,\eta) = (\Delta' + r\,\mathbf{b}_r' + z\,\mathbf{b}_z' + h\,\gamma')\,\bar{\mathbf{U}} \tag{1.3}$$

where

$$\Delta' = \frac{1}{4}[\,\mathbf{t}' - r_0\,\mathbf{b}_r' - z_0\,\mathbf{b}_z'\,] \tag{1.4a}$$

$$\gamma' = \frac{1}{4}[\,\mathbf{h}' - (\mathbf{h}'\mathbf{R})\,\mathbf{b}_r' - (\mathbf{h}'\mathbf{Z})\,\mathbf{b}_z'\,] \tag{1.4b}$$

and

$$\bar{\mathbf{U}}^t = < U_1, U_2, U_3, U_4 > \tag{1.4c}$$

with

$$\begin{aligned}
\mathbf{t}^t &= < 1, 1, 1, 1 > \\
\mathbf{h}^t &= < 1, -1, 1, -1 > \\
\mathbf{R}^t &= < r_1, r_2, r_3, r_4 > \\
\mathbf{Z}^t &= < z_1, z_2, z_3, z_4 > \\
\mathbf{b}_{rI} &= \frac{\partial \mathrm{N}_I}{\partial r} \Big|_{\xi = \eta = 0} \\
\mathbf{b}_{zI} &= \frac{\partial \mathrm{N}_I}{\partial z} \Big|_{\xi = \eta = 0} \\
r_0 &= \frac{1}{4}(r_1 + r_2 + r_3 + r_4) \\
z_0 &= \frac{1}{4}(z_1 + z_2 + z_3 + z_4)
\end{aligned} \tag{1.5}$$

where

$$h = \xi\, \eta \tag{1.6}$$

This form is particularly useful in subsequent calculations where derivatives of the shape functions are involved. It can be shown that the derivatives of the first three terms of the alternative form of the shape function are constant and the partial derivatives of h are given by

$$\begin{Bmatrix} \frac{\partial h}{\partial r} \\ \frac{\partial h}{\partial z} \end{Bmatrix} = \frac{1}{J} \begin{bmatrix} zt & -zs \\ -rt & rs \end{bmatrix} \begin{Bmatrix} \eta \\ \xi \end{Bmatrix} \tag{1.7}$$

where the area integrals of the derivatives of h have the property

$$\int_{\Omega_e} h_{,r}\, d\Omega = \int_{\Omega_e} h_{,z}\, d\Omega = 0 \tag{1.8}$$

and are thus orthogonal to a constant on any quadrilateral element.

In the following discussion the torsionless axisymmetric problem is considered where

$$\boldsymbol{\sigma}^t = [\sigma_r, \sigma_z, \sigma_{rz}, \sigma_\theta] \tag{1.9}$$

are the stress components which enter the internal energy; and

$$\boldsymbol{\epsilon}^t = [\epsilon_r, \epsilon_z, \epsilon_{rz}, \epsilon_\theta] \tag{1.10}$$

are the associated strain components which are related to the displacement field through

$$\boldsymbol{\epsilon}^t = \boldsymbol{\epsilon}\,(u)^t = [\, u_{r,r}, u_{z,z}, u_{r,z} + u_{z,r}, \frac{u_r}{r}] \tag{1.11}$$

Using (1.3), the gradient of the displacements may be written as

$$\boldsymbol{\epsilon}^t = \mathbb{B}\, \mathbf{d} \tag{1.12}$$

where

$$\mathbf{d} = \begin{Bmatrix} \mathbf{u}_r \\ \mathbf{u}_z \end{Bmatrix} \tag{1.13}$$

is the element nodal displacement vector, and

$$\mathbf{B} = \begin{bmatrix} \mathbf{b}_r^t & 0 \\ 0 & \mathbf{b}_z^t \\ \mathbf{b}_z^t & \mathbf{b}_r^t \\ 0 & 0 \end{bmatrix} + \begin{bmatrix} h_{,r}\,\boldsymbol{\gamma}^t & 0 \\ 0 & h_{,z}\,\boldsymbol{\gamma}^t \\ h_{,z}\,\boldsymbol{\gamma}^t & h_{,r}\,\boldsymbol{\gamma}^t \\ \dfrac{\mathbf{N}}{r} & 0 \end{bmatrix} \tag{1.14}$$

is the strain-displacement matrix. The first term in the split of the strain-displacement matrix is derived from the first three terms in (1.3) (excluding the ϵ_θ term) and is constant over the element. The second term results from the derivatives of h and the ϵ_θ term.

For a linear elastic isotropic material the material, modulus matrix $\mathbb{D}$ may be expressed as

$$\mathbf{D} = \begin{bmatrix} D_{11} & D_{12} & 0 & D_{14} \\ D_{21} & D_{22} & 0 & D_{24} \\ 0 & 0 & D_{33} & 0 \\ D_{41} & D_{42} & 0 & D_{44} \end{bmatrix} \tag{1.15}$$

where

$$D_{ii} = \lambda + 2\mu \; ; D_{ij} = \lambda \; ; D_{33} = \mu \qquad i,j = 1, 2, 4 \; ; \; i \neq j \tag{1.16}$$

The Lamé parameters λ and μ may also be expressed in terms of Young's modulus, E, and Poisson's ratio, ν, as

$$\lambda = \frac{\nu E}{(1+\nu)(1-2\nu)} \tag{1.17a}$$

and

$$\mu = \frac{E}{2(1+\nu)} \tag{1.17b}$$

Subsequent development also requires the inverse of $\mathbb{D}$, which may be written as

$$\mathbf{C} = \mathbf{D}^{-1} = \begin{bmatrix} C_{11} & C_{12} & 0 & C_{14} \\ C_{21} & C_{22} & 0 & C_{24} \\ 0 & 0 & C_{33} & 0 \\ C_{41} & C_{42} & 0 & C_{44} \end{bmatrix} \tag{1.18}$$

For the linear isotropic case, $D_{ij} = D_{ji}$, $D_{11} = D_{22} = D_{44}$ and $D_{12} = D_{14} = D_{24}$. Thus the elements of the C matrix are given by ($\mathbf{C}_{ij} = \mathbf{C}_{ji}$)

$$C_{33} = \frac{1}{D_{33}}$$

$$C_{12} = C_{14} = C_{24} = \frac{-D_{12}}{D_{11}(D_{11} + D_{12}) - 2D_{12}^2} \tag{1.19}$$

$$C_{ii} = \frac{1 - 2D_{12}C_{12}}{D_{11}} \; ; \qquad i = 1, 2, 4$$

Finally, it is useful to write the Jacobian in the following form, after Zienkiewicz [1977],

$$J(\xi, \eta) = J_0 + J_1\xi + J_2\eta \tag{1.20}$$

where

$$J_0 = rs \cdot zt - rt \cdot zs$$
$$J_1 = rs \cdot zh - rh \cdot zs \tag{1.21}$$
$$J_2 = rh \cdot zt - rt \cdot zh$$

with

$$rs = \frac{1}{4}(-r_1 + r_2 + r_3 - r_4)$$
$$rt = \frac{1}{4}(-r_1 - r_2 + r_3 + r_4)$$
$$rh = \frac{1}{4}(+r_1 - r_2 + r_3 - r_4) \tag{1.22}$$
$$zs = \frac{1}{4}(-z_1 + z_2 + z_3 - z_4)$$
$$zt = \frac{1}{4}(-z_1 - z_2 + z_3 + z_4)$$
$$zh = \frac{1}{4}(+z_1 - z_2 + z_3 - z_4)$$

2. Element Stiffness Formulation via the Hellinger-Reissner Variational Principle

The element stiffness matrix is formulated using the Hellinger-Reissner variational principle. The stress field presented by Pian & Sumihara [1984] for the plane stress, plane strain element is modified to obtain the correct rank for the axisymmetric element. The plane strain, plane stress formulation yielded excellent results for all Poisson ratios as well as for bending problems. The modified stress field, for the axisymmetric element, is designed to retain these properties.

The Hellinger-Reissner functional for a linear elastic material can be written as

$$\Pi_R = \int_{\Omega_e} [-\frac{1}{2}\sigma^t \mathbf{C}\sigma + \sigma^t \epsilon(u)] r \, d\Omega - \int_{\partial\Omega_e} u^t \bar{t} r \, d\Gamma \tag{2.1}$$

The first variation yields a formulation which includes the constitutive equation and the momentum balance equation and is given by

$$\delta\Pi_R = \int_{\Omega_e} [\delta\sigma^t (-\mathbf{C}\sigma + (\epsilon(u))^t) + \delta(\epsilon(u))^t \sigma] r \, d\Omega - \int_{\partial\Omega} \delta u^t \bar{t} r \, d\Gamma = 0 \tag{2.2}$$

The construction of a finite element model requires an approximation of the displacements and the stresses. The dispacement field may be approximated using (1.3). Let the stress field be of the form

$$\sigma = \mathbf{S}\, s \tag{2.3}$$

Substituting (1.3) and (2.3) into (2.2) yields the finite element approximation of the variational equation, given by

$$\delta\Pi_R = -\delta s^t (\mathbf{H}s - \mathbf{G}d) + \delta d^t (\mathbf{G}^t s - \mathbf{f}) = 0 \tag{2.4}$$

where

$$\mathbf{G} = \int_{\Omega_e} \mathbf{S}^t B \, r \, d\Omega \tag{2.5}$$

$$\mathbf{H} = \int_{\Omega_e} \mathbf{S}^t \mathbf{C}\mathbf{S} r d\Omega \tag{2.6}$$

The stress field proposed by Pian & Sumihara [1984] is modified to obtain a correct rank for the torsionless axisymmetric problem. The plane stress/strain element has three rigid body modes. In the axisymmetric case only one rigid body mode is present, the translation in the z direction. A translation in the r direction introduce hoop stresses. Thus, only the rigid body rotation appears as a

spurious zero energy mode if σ_θ is assumed constant over the element domain. This suggests allowing linear variation in σ_θ in the r and z directions or at least in one direction. The variation is taken in the global frame in order to obtain a frame invariant element (even if σ_θ is allowed to vary only in one direction). This leads to the following stress field

$$\sigma = \begin{Bmatrix} \sigma_r \\ \sigma_z \\ \sigma_{rz} \\ \sigma_\theta \end{Bmatrix} = \begin{bmatrix} 1 & 0 & 0 & 0 & rs^2\bar{\eta} & rt^2\bar{\xi} & 0 & 0 \\ 0 & 1 & 0 & 0 & zs^2\bar{\eta} & zt^2\bar{\xi} & 0 & 0 \\ 0 & 0 & 1 & 0 & rs\,zs\,\bar{\eta} & rt\,zt\,\bar{\xi} & 0 & 0 \\ 0 & 0 & 0 & 1 & 0 & 0 & \bar{r} & \bar{z} \end{bmatrix} \begin{Bmatrix} \bar{\sigma}_r \\ \bar{\sigma}_z \\ \bar{\sigma}_{rz} \\ \bar{\sigma}_\theta \\ Q_r \\ Q_z \\ Q_{r\theta} \\ Q_{z\theta} \end{Bmatrix} = \mathbf{S}\,s \tag{2.7}$$

where

$$\bar{r} = rs\,\bar{\xi} + rt\,\bar{\eta} + rh\,\bar{h} \tag{2.8a}$$

$$\bar{z} = zs\,\bar{\xi} + zt\,\bar{\eta} + zh\,\bar{h} \tag{2.8b}$$

and

$$\bar{\xi} = \xi - \xi_0 \;\; ; \;\; \bar{\eta} = \eta - \eta_0 \;\; ; \;\; \bar{h} = h - h_0 \tag{2.9}$$

η_0 , ξ_0 and h_0 are shifts introduced in order to make H block diagonal. In order to obtain this result the following requirement must be meet.

$$\begin{aligned} \int_{\Omega_e} \bar{\xi} r \, d\Omega = 0 \\ \int_{\Omega_e} \bar{\eta} r \, d\Omega = 0 \\ \int_{\Omega_e} \bar{h} r \, d\Omega = 0 \end{aligned} \tag{2.10}$$

The resulting ξ_0 η_0 and $\mathbf{h}_0$ are given by

$$\xi_0 = \frac{\sum_{I=1}^{4} \left(J_1 + J_0 \xi_I + \frac{1}{3} J_2 \xi_I \eta_I \right) r_I}{\alpha} \tag{2.11a}$$

$$\eta_0 = \frac{\sum_{I=1}^{4} \left(J_2 + J_0 \eta_I + \frac{1}{3} J_1 \xi_I \eta_I \right) r_I}{\alpha} \tag{2.11b}$$

$$h_0 = \frac{\sum_{I=1}^{4} \left(\xi_I \eta_I J_0 + \eta_I J_1 + \xi_I J_2 \right) r_I}{3\alpha} \tag{2.11c}$$

with

$$\alpha = \sum_{I=1}^{4} \left(3J_0 + J_1 \xi_I + J_2 \eta_I \right) r_I \tag{2.12}$$

The stationary condition (2.4) becomes

$$\mathbf{H}\,s = \mathbf{G}\,d \tag{2.13a}$$

$$\mathbf{G}^t \, s = \mathbf{f} \tag{2.13b}$$

Combining (2.13a) and (2.13b) yields the element stiffness matrix given by

$$K_e = \mathbf{G}^t \, \mathbf{H}^{-1} \, \mathbf{G} \tag{2.14}$$

where G and H are given in explicit form in appendix A.

From a strict point of stabilizing the element, seven parameters would suffice (Pian & Chen [1983]). Thus, either $Q_{r\theta}$ or $Q_{z\theta}$ can be set to zero. In this case, only a (3x3) stabilization matrix is inverted. In plate bending applications it is better to omit $Q_{r\theta}$. The resulting element, requires at least two elements in the r-direction any time there is a change in σ_θ in the r-direction. For clarification, let the eight parameter element be denoted as the full stress field (FSF) element and the seven parameter one as the degenerated stress field (DSF) element.

REMARK 2.1 : The shift introduced by $\bar{\xi}$, $\bar{\eta}$ and $\bar{h}$ makes the H matrix block diagonal. Thus, it is necessary to invert a (4X4) matrix for the FSF element, but only (3X3) matrix for the DSF element.

REMARK 2.2 : The stiffness matrix of the two-dimensional element presented by Pian & Sumihara [1984] can be written as the sum of the uncoupled under-integrated stiffness matrix and the stabilization matrix. This leads to a very efficient implementation from a computational point of view (about 40% of the computation required for the fully-integrated isoparametric axisymmetric element.). Due to the curvilinear coordinate in the r-direction, this decoupling is not possible in the axisymmetric case. As a result, the cost of computing the element stiffness matrix is about the same as for the fully-integrated isoparametric axisymmetric element.

3. Numerical Results

A number of examples are given to compare the proposed elements with the usual displacement method , 2X2 quadrature isoparametric element (referred to as the 2X2 element) and where available with results from Bachrach & Belytschko [1986] (OABI element). Results for all examples are normalized by an exact solution.

Five examples are reported. The first example a thick-walled cylinder subjected to uniform internal pressure. Axisymmetric plate subjected to uniform normal loading is investigated in the second example. The third example is a cylindrical shell loaded by an edge moment. The fourth example is a thin sphere subjected to an internal pressure. The fifth example is a thick sphere subjected to an internal pressure.

Example 3.1

The thick-walled cylinder subjected to internal pressure problem, proposed by MacNeal & Harder [1985] as a standard problem is addressed first. The problem parameters are : $r_{in} = 3.0$, $r_{out} = 9.0$, $z_{bottom} = 0$, $z_{top} = 1.0$, $E = 1000$ and the loading is an unit internal pressure. The mesh consists of five elements in the r-direction and 1 in the z-direction. The problem is analyzed once for a regular mesh Fig. 3.1a and once using a skewed mesh Fig. 3.1b ($\theta_1 = 21.801^o$ and $\theta_2 = 45.0^o$). The analytical solution is given in MacNeal & Harder [1985]. The displacement at point A for the various formulations is given in Table 1. The regular mesh results show that the DSF element gives the exact result at each node (it is noted that the exact result is obtained using one DSF element). The FSF element has about 1.5% error in the worst case. For the skewed mesh again the DSF element shows the lowest error less than 0.5%; however, the FSF element has about 2.5% error in the worst case. For both meshs the 2X2 element yields good results for the low values on Poisson's ratio, but as expected locks as the incompressible limit is approached.

Table 1. MacNeal-Harder test						
ν	Regular mesh			Skewed mesh		
	FSF	DSF	2X2	FSF	DSF	2X2
0.	0.99363	1.00000	0.99363	0.98488	0.99695	0.98869
0.3	0.99035	1.00000	0.98820	0.98071	0.99697	0.98218
0.49	0.98623	1.00000	0.84650	0.97605	0.99696	0.81615
0.499	0.98596	1.00000	0.35908	0.97575	0.99695	0.31467
0.4999	0.98593	1.00000	0.05313	0.97572	0.99659	0.04370

Example 3.2

The performance of each element in plate bending problems is addressed next. First a simply supported circular plate is subjected to an uniform unit normal load. The problem parameters are : the plate radius, $R = 10$, the plate depth, $h = 1.$, and Young's modulus, $E = 1875$. The analytical solution for a uniformly loaded, thick or thin circular plate with simple supports is given in Timoshenko & Woinowsky-Krieger [1959]. The mesh consists of four elements in the r-direction and 1 in the z-direction. A regular mesh Fig 3.2a and a skewed mesh Fig 3.2b ($\theta = 26.265^o$) are used. The displacement of point A for each case is summarized in Table 2. The DSF and FSF elements are identical when a regular mesh is used; however, the DSF element is slightly more accurate when the skewed mesh is used. It is noted that when the skewed mesh is used the performance of both elements improves as the ν approaches 0.5 (e.g., from an error of about 15% to about 3%). Both elements show a large advantage over the 2X2 element for all values of ν. This is expected since the 2X2 element is known to be overstiff in the bending mode. Both elements yield better results in comparison with the OABI element. The advantage increases as ν approaches 0.5. While the proposed element's performance is independent of ν the OABI element is not.

Table 2. Plate under normal load							
ν	Regular mesh				Skewed mesh		
	FSF	DSF	2x2	OABI	FSF	DSF	2X2
0.	1.02470	1.02470	0.67555	-	0.85328	0.85438	0.57400
0.25	1.02540	1.02541	0.68799	1.05	0.91316	0.91513	0.61117
0.30	1.02718	1.02718	0.64493	-	0.92399	0.92621	0.58294
0.49	1.02605	1.02606	0.07770	-	0.96496	0.96786	0.08608
0.499	1.02607	1.02608	0.02137	-	0.96698	0.96987	0.02275
0.4999	1.02607	1.02608	0.01546	1.13	0.96718	0.97008	0.01625

It is of interest to examine the sensitivity of the proposed elements with changes in the plate depth. Only the regular mesh is considered (Fig 3.2a). First, the plate depth is decreased to 0.5 and the displacement at point A is given in Table 3. The FSF and DSF elements show excellent results. It is noted that both formulations yield identical results. The 2X2 element, on the other hand, yields very poor results. The OABI element is outperformed by both the FSF and DSF elements. The plate thickness is then increased to 2.5 . The displacement of point A is summarized in Table 3. The DSF and FSF elements show almost identical results with DSF element showing again a small advantage. The 2X2 element yields relatively good results for the low ν ratio. The OABI yields about the same results as the proposed elements, however, note that for low values of ν it is flexible while for values of ν approaching 0.5 it is stiff. It is noted that the performance of both the FSF and DSF elements is almost independent of the plate depth and ν Thus, these elements are applicable to both thick and thin plates, for all values of ν.

Table 3. Plate thickness variation

ν	h = 0.5				h = 2.5			
	FSF	DSF	*OABI*†	2x2	FSF	DSF	*OABI*†	2X2
0.	1.02653	1.02653	-	0.35265	1.01823	1.01823	-	0.93003
0.25	1.02708	1.02708	0.992	0.43360	1.02116	1.02128	1.05	0.83512
0.30	1.02718	1.02718	-	0.43024	1.02175	1.02191	-	0.76415
0.49	1.02756	1.02756	-	0.06530	1.02412	1.02447	-	0.14579
0.499	1.02758	1.02758	-	0.01037	1.02425	1.02460	-	0.09198
0.4999	1.02758	1.02758	1.04	0.00441	1.02426	1.02460	1.12	0.08578

Example 3.3

The purpose of this example is to test the performance of the proposed elements on a problem where σ_θ varies in the r-direction. A problem with this property, suggested by Bachrach & Belytschko [1986], is a cylindrical shell which is modeled by 17 elements in the z-direction 1 element in the r-direction, see Fig. 3.3. The aspect ratio of the elements is 3 (i.e., $\Delta z / \Delta r = 3$). The problem parameters are : Median radius, $a = 167.5$, Youngs modulus is $E = 11250.$, the cylinder thickness is $h = 1$, and the applied end moment $M = 2000$ per unit length. The analytical results are based on an infinitely long thin shell solution given in Timoshenko & Woinowsky-Krieger [1959].

The displacement of point A is summarized in Table 4. As expected the FSF element performs very well with a tip displacement error less than 1.6%. The DSF element performs well for $\nu = 0$, about 1.6% tip displacement error; however, as ν approaches 0.5 the tip displacement error grows to 13.6% for $\nu = 0.4999$. This results for the DSF element is consistent with the fact that the element cannot account for variations in σ_θ in the r-direction. To verify this conclusion, the mesh is refined in the r-direction. The modified mesh consists of 17 elements in the z-direction and 2 in the r-direction. The result is presented in the column under *DSF**. As expected the largest tip displacement error is reduced to 1.5%. The OABI yields similar results to the FSF element, while the 2X2 element is outperformed by a large margin (even by the DSF element with only one element in the r-direction).

Table 4. Infinite Cylinder

ν	FSF	DSF	*DSF**	OABI	2X2
0.	0.98464	0.98051	0.98464	-	0.41994
0.25	0.98414	1.01649	0.99152	1.01	0.46419
0.30	0.98411	1.03165	0.99485	-	0.47047
0.49	0.98423	1.12857	1.01397	-	0.24025
0.499	0.98424	1.13522	1.01515	-	0.08112
0.4999	0.98424	1.13590	1.01527	1.02	0.01412

Example 3.4

A thin sphere problem subjected to internal pressure is addressed. The analytical solution for a thin or thick sphere is given by Roark & Young [1975]. The problem is shown in Fig 3.4a. The problem parameters are : mean radius, $a = 9.5$, the sphere thickness is, $h = 1.$, and Young's modulus is, $E = 1000$. A unit internal pressure is applied. Only ten elements are used in this mesh. The resulting displacements at points A and B are summarized in Table 5. For low values of ν the best result is given by the 2X2 element (the best symmetry obtained). However, as ν approaches 0.5 the 2X2 element locks. The two elements proposed follow the 2X2 element very closely for the low values of ν, with the DSF element, again, yielding slightly better results. However, the elements do not lock at the nearly incompressible limit.

† results reported for the OABI element are obtained using 10 elements in the r-direction and 1 in the z-direction.

Table 5. Thin Sphere "old" load						
ν	A			B		
	FSF	DSF	2x2	FSF	DSF	2X2
0.	1.06123	1.05892	1.02354	0.99375	0.99477	0.99656
0.3	1.07623	1.07360	1.02653	0.99009	0.99192	0.99174
0.49	1.08475	1.08541	0.89644	0.98446	0.98800	0.87576
0.499	1.08506	1.08604	0.42394	0.98405	0.98772	0.41850
0.4999	1.08510	1.08610	0.06768	0.98401	0.98770	0.06733

For the shell like sphere case Halleux [1980] suggested that the nodal forces be computed using shape functions of the form given in Fig. 3.4b. All three elments yield better results with loads computed in this way. Again for the low values of ν the 2X2 yields the best results, and the DSF element is slightly superior to the FSF element.

Table 6. Thin Sphere "new" load						
ν	A			B		
	FSF	DSF	2x2	FSF	DSF	2X2
0.	1.02186	1.01946	0.99151	0.99528	0.99630	0.99820
0.3	1.02494	1.02172	0.98551	0.98999	0.99184	0.99179
0.49	1.02481	1.02370	0.87427	0.98269	0.98626	0.87588
0.499	1.02469	1.02381	0.41281	0.98218	0.98589	0.41844
0.4999	1.02467	1.02382	0.06273	0.98213	0.98585	0.06544

Example 3.5

A thick sphere problem is addressed. The problem parameters are : $r_{in} = 1.$, $r_{out} = 5.$ and the Young's modulus is, $E = 1000$. The mesh used is ten elements in the circumferential direction and four in the radial direction. The mesh is shown in Fig. 3.5. The analytical solution is given by Roark & Young [1975]. The results for the displacements of points A and B are summarized in Table 7. The best results are obtained by the DSF element. The 2X2 and the FSF yield results which are almost as good for the low values of ν, but at the nearly incompressible limit the FSF element yields slightly better results than the DSF element and the 2X2 element locks.

Table 7. Thick Sphere						
ν	A			B		
	FSF	DSF	2x2	FSF	DSF	2X2
0.	0.97467	0.96934	0.96385	0.94756	0.95782	0.94808
0.3	0.94910	0.94898	0.92714	0.92804	0.94963	0.91279
0.49	0.92016	0.92727	0.42590	0.90397	0.94273	0.42190
0.499	0.91830	0.92584	0.06945	0.90237	0.94237	0.06924
0.4999	0.91811	0.92569	0.00740	0.90220	0.94233	0.00740

4. Conclusion

Axisymmetric elements based on the Hellinger-Reissner variational principle are presented. The elements presented possess the correct rank, are frame invariant, perform well for all Poisson's ratios and yield excellent results for bending problems.

The γ projection operator and the stress fields used lead to an elegant formulation of the stiffness matrix for both elements presented. An important computational aspect of this formulation is that only small matrices need to be inverted ((4x4) for the FSF element and (3x3) for the DSF element).

The DSF element uses only seven independent interpolants, i.e. the minimum independent interpolants required to obtain correct rank. Although this element is of the correct rank, it requires

at least two elements in the r-direction any time there is a variation of the σ_θ in the r-direction, as could be seen in example 3.

The computation cost difference between the FSF and the DSF elements is very small. It is also noted that in most examples presented (with the exception of example 3) the difference between the two formulations lead to very small difference in the results. In all examples both formulations show a clear superiority over the fully-integrated isoparametric element.

The decoupling of the stiffness matrix into an under-integrated stiffness matrix and a stabilization stiffness matrix in the plane stress, plane strain formulation does not carry over to the axisymmetric case. Thus, no computation efficiency is gained over the fully-integrated isoparametric axisymmetric element.

Acknowledgments

We wish to thank Timothy Guinane and Ariel Reich for their help.

REFERENCES

Bachrach, W.E. & T. Belytschko, [1986], "Axisymmetric elements with high coarse-mesh accuracy", *Computers & Structures, Vol. 23, No. 3, pp. 323-331.*

Belytschko, T. & W.E. Bachrach, [1986], "Efficient implementation of Quadrilaterals with high coarse-mesh accuracy", *Computer Methods in Applied Mechanics and Engineering, Vol. 54, pp. 279-301.*

Belytschko, T., J.S.-J. Ong, W.K Liu & J.M. Kennedy [1984], "Hourglass control in linear and nonlinear problems", *Computer Methods in Applied Mechanics and Engineering, Vol. 43, pp. 251-276.*

Bicanic, N. & E. Hinton, [1979], "Spurious modes in two-dimensional isoparametric elements", *International Journal for Numerical Methods in Engineering, Vol. 14, pp. 1545-1557.*

Flanagan, D.P., & T. Belytschko, [1981], "A uniform strain hexahedron and quadrilateral with orthogonal hourglass control", *International Journal for Numerical Methods in Engineering, Vol. 17, pp. 679-706.*

Halleux, J.P., [1980], "Transient non-linear analysis of thin axisymmetric structure", *Numerical Methods for Non-Linear Problems (Eds. C. Taylor, E. Hinton and D. R.J. Owen) Vol. 1, Pineridge Press, Swansea.*

Hughes, T.J.R., [1977], "Equivalence of finite elements for nearly incompressible elasticity", *Journal of Applied Mechanics, Vol. 44, pp. 181-183.*

Hughes, T.J.R., [1980], "Generalization of selective integration procedures to anisotropic and nonlinear media", *International Journal for Numerical Methods in Engineering, Vol. 15, pp. 1413-1418.*

Hughes, T.J.R., [1987], The Finite Element Method, *Prentice-Hall, Inc., Englewood Cliffs, New Jersey.*

Lax, P.D. & R.D. Richtmyer, [1956], "Survey of the stability of linear finite difference equations", *Communications in Pure and Applied Mathematics, Vol. 9, pp. 267.*

Liu, W.K. & T. Belytschko, [1984], "Efficient linear and nonlinear heat conduction with a quadrilateral element", *International Journal for Numerical Methods in Engineering, Vol. 20, pp. 931-948.*

MacNeal, R.H. & R.L. Harder, [1985], "A proposed standard set of problems to test finite element accuracy", *Finite Elements in Analysis and Design, Vol. 1, pp. 3-20.*

Malkus, D.S. & T.J.R. Hughes, [1978], "Mixed finite element methods - Reduced and selective integration techniques: A unification of concepts", *Computer methods in applied mechanics and Engineering, Vol. 15, pp. 63-81.*

Pian, P.H.H. & D. Chen, [1983], "On the suppression of zero energy deformation modes", *International Journal for Numerical Methods in Engineering, Vol. 19, pp. 1741-1752.*

Pian, P.H.H. & K. Sumihara, [1984], "Rational approach for assumed stress finite elements", *International Journal for Numerical Methods in Engineering, Vol. 20, pp. 1685-1695.*

Roark, R.J. & W.C. Young, [1975], Formulas for stress and strain, *McGraw-Hill, New-York.*

Simo, J.C., R.L. Taylor & K.S. Pister, [1985], "Variational and projection methods for the volume constraint in finite deformation elasto-plasticity", *Computer Methods in Applied Mechanics and Engineering, Vol. 51, pp. 177-208.*

Timoshenko, S. & J.N. Goodier, [1970], Theory of Elasticity, *McGraw-Hill, New-York.*

Timoshenko, S. & S. Woinowsky-Krieger, [1959], Theory of Plates and Shells, *McGraw-Hill, New-York.*

Zienkiewicz, O.C., [1977], The Finite Element Method, *3rd ed., MacGraw-Hill Book Co., London.*

Appendix A : Explicit form of G and H

The **G** and **H** defined in section 2 matrices are given in an explicit form. The format presented in this appendix is for the FSF element. To obtain these matrices for the DSF element the appropriate lines and rows must be deleted. It is also noted that all the required quantities can be computed explicitly.

Substituting the stress field given by (2.7) into (2.5) yields the **G** given by

$$\mathbf{G} = \begin{bmatrix} b_r^I V & 0 \\ 0 & b_z^I \\ b_z^I V & b_r^I \\ 0 & 0 \\ 0 & 0 \\ 0 & 0 \\ 0 & 0 \\ 0 & 0 \end{bmatrix} + \begin{bmatrix} L_r \gamma^I & 0 \\ 0 & L_z \gamma^I \\ L_z \gamma^I & L_r \gamma^I \\ I_n & 0 \\ (rs^2 L_{\eta r} + rs\, zs\, L_{\eta z}) \gamma^I & (zs^2 L_{\eta z} + rs\, zs\, L_{\eta r}) \gamma^I \\ (rt^2 L_{\xi r} + rt\, zt\, L_{\xi z}) \gamma^I & (zt^2 L_{\xi z} + zt\, rt\, L_{\xi r}) \gamma^I \\ rs\, \bar{N}_\xi + rt\, \bar{N}_\eta + rh\, \bar{N}_{\xi\eta} & 0 \\ zs\, \bar{N}_\xi + zt\, \bar{N}_\eta + zh\, \bar{N}_{\xi\eta} & 0 \end{bmatrix} \tag{A.1}$$

where

$$\bar{N}_\eta = \int_{\Omega_e} \mathrm{N}_I\, \bar{\eta}\, d\Omega \quad ; \quad \bar{N}_\xi = \int_{\Omega_e} \mathrm{N}_I\, \bar{\xi}\, d\Omega \quad ; \quad \bar{N}_{\xi\eta} = \int_{\Omega_e} \mathrm{N}_I\, \bar{h}\, d\Omega \tag{A.2}$$

$$I_n = \int_{\Omega_e} \mathrm{N}_I\, d\Omega \tag{A.3}$$

$$\begin{aligned} L_r &= \int_{\Omega_e} h_{,r}\, r\, d\Omega \quad ; \quad L_z = \int_{\Omega_e} h_{,z}\, r\, d\Omega \\ L_{\eta r} &= \int_{\Omega_e} \bar{\eta} h_{,r}\, r\, d\Omega \quad ; \quad L_{\eta z} = \int_{\Omega_e} \bar{\eta} h_{,z}\, r\, d\Omega \\ L_{\xi r} &= \int_{\Omega_e} \bar{\xi} h_{,r}\, r\, d\Omega \quad ; \quad L_{\xi z} = \int_{\Omega_e} \bar{\xi} h_{,z}\, r\, d\Omega \end{aligned} \tag{A.4}$$

Note that (A.2) through (A.4) can be integrated explicitly.

Substituting the stress field given by (2.6) into (2.5) yields **H** of the form

$$\mathbf{H} = \begin{bmatrix} \mathbf{H}^I & 0_{4x4} \\ 0_{4x4} & \mathbf{H}^{II} \end{bmatrix} \tag{A.5}$$

where

$$\mathbf{H}^I = \mathbf{C}\, V \tag{A.6}$$

with V the element volume. The elements of the (4x4) $\mathbf{H}^{II}$ are given by (recall that H is symmetric)

$$
\begin{aligned}
\mathbf{H}^{II}_{11} &= [\, rs^4 C_{11} + zs^4 C_{22} + rs^2 zs^2 \,(\, C_{12} + C_{21} + C_{33} \,)\,]\, I_1 \\
\mathbf{H}^{II}_{12} &= [\, rs^2 \,(\, rt^2 C_{11} + zt^2 C_{12} \,) + zs^2 \,(\, rt^2 C_{21} + zt^2 C_{22} \,) + rs\ rt\ zs\ zt\ C_{33} \,]\, I_2 \\
\mathbf{H}^{II}_{13} &= [\, rs\, I_3 + zt\, I_1 + rh\, I_5 \,]\, rs^2 C_{41} + [\, rs\, I_3 + rt\, I_1 + rh\, I_5 \,]\, zs^2 C_{42} \\
\mathbf{H}^{II}_{14} &= [\, zs\, I_3 + zs\, I_1 + zh\, I_5 \,]\, rs^2 C_{41} + [\, zs\, I_3 + zt\, I_1 + zh\, I_5 \,]\, zs^2 C_{42} \\
\mathbf{H}^{II}_{22} &= [\, rt^4 C_{11} + rt^2 zt^2 \,(\, C_{12} + C_{21} + C_{33} \,) + zt^4 C_{22} \,]\, I_2 \\
\mathbf{H}^{II}_{23} &= [\, rs\, I_2 + rt\, I_3 + rh\, I_4 \,]\, rs^2 C_{41} + [\, rs\, I_2 + rt\, I_3 + rh\, I_4 \,]\, zt^2 C_{42} \\
\mathbf{H}^{II}_{24} &= [\, zs\, I_2 + zt\, I_3 + zh\, I_4 \,]\, rt^2 C_{41} + [\, zs\, I_2 + zt\, I_3 + zh\, I_4 \,]\, zt^2 C_{42} \\
\mathbf{H}^{II}_{33} &= (\, rs^2 I_2 + 2\,(\, rs\ rt\, I_3 + rs\ rh\, I_4 + rt\ rh\, I_5 \,) + rt^2 I_1 + rh 2 I_6 \,)\, C_{44} \\
\mathbf{H}^{II}_{34} &= [\,(\, zs\, I_2 + zt\, I_3 + zh\, I_4 \,)\, rs + (\, zs\, I_3 + zt\, I_1 + zh\, I_5 \,)\, rt + \\
&\qquad (\, zs\, I_4 + zt\, I_5 + zh\, I_6 \,)\, rh \,]\, C_{44} \\
\mathbf{H}^{II}_{44} &= (\, zs^2 I_2 + 2\,(\, zs\ zt\, I_3 + zs\ zh\, I_4 + zt\ zh\, I_5 \,) + zt^2 I_1 + zh^2 I_6 \,)\, C_{44}
\end{aligned}
\tag{A.7}
$$

where

$$
\begin{aligned}
I_1 &= \int_{\Omega_e} \bar{\eta}^2 r \, d\Omega \quad ; \quad I_2 = \int_{\Omega_e} \bar{\xi}^2 r \, d\Omega \\
I_3 &= \int_{\Omega_e} \bar{\xi}\bar{\eta} r \, d\Omega \quad ; \quad I_4 = \int_{\Omega_e} \bar{\xi}\bar{h} r \, d\Omega \\
I_5 &= \int_{\Omega_e} \bar{\eta}\bar{h} r \, d\Omega \quad ; \quad I_6 = \int_{\Omega_e} \bar{h}\bar{h} r \, d\Omega
\end{aligned}
\tag{A.8}
$$

Note that (A.8) can be computed explicitly.

Figure Captions

Figure 1.1. Local node ordering.

Figure 3.1a. Thick-cylinder, regular mesh.

Figure 3.1b. Thick-cylinder, skewed mesh.

Figure 3.2a. Simply supported circular plate, regular mesh.

Figure 3.2b. Simply supported circular plate, skewed mesh.

Figure 3.3. Cylinderical thin-shell loaded by an edge moment.

Figure 3.4a. Thin-sphere mesh.

Figure 3.4b. Halleux's shape functions for computing the nodal loads for an axisymmetric shell.

Figure 3.5. Thick-sphere mesh.

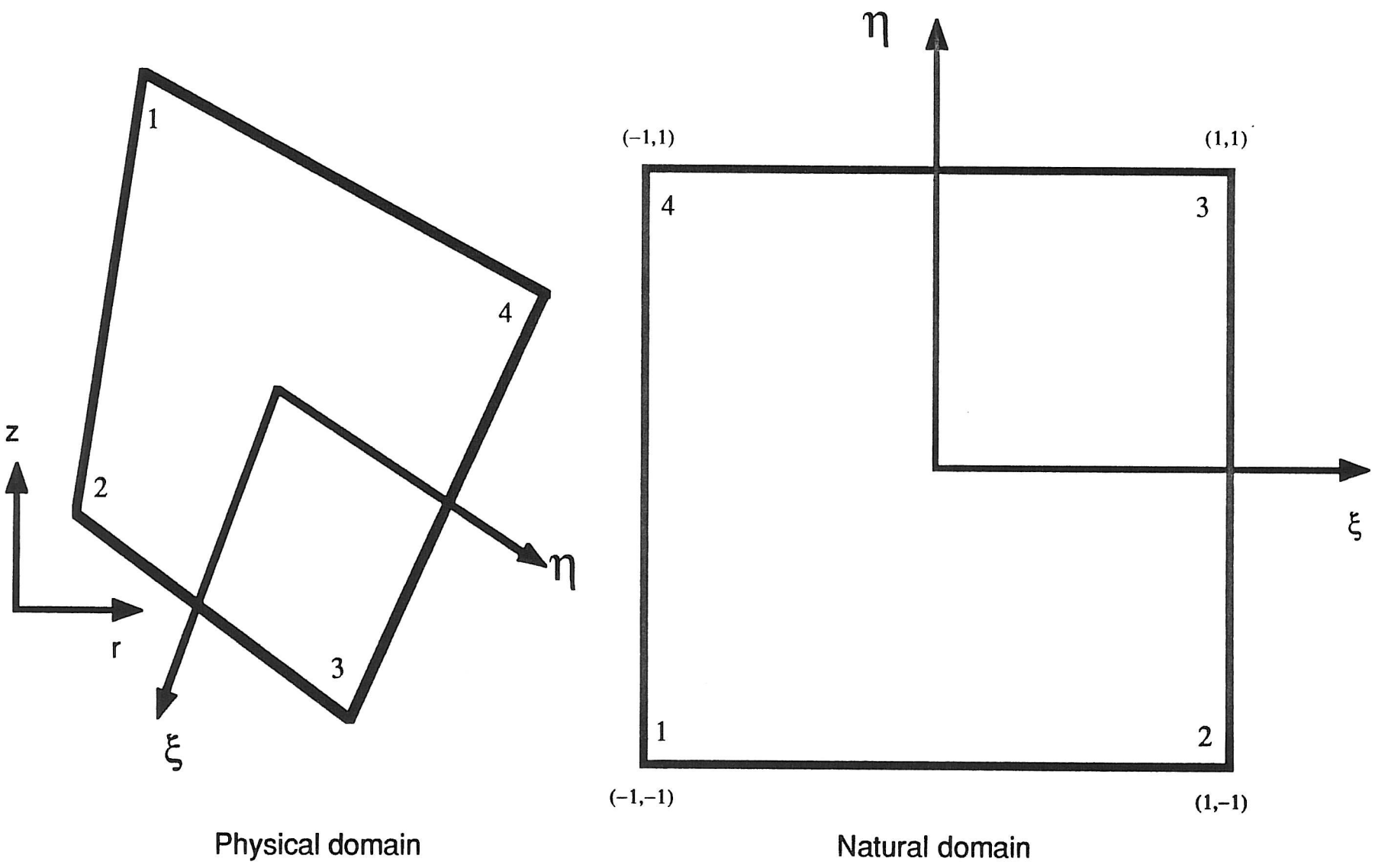

Figure 1.1 Local node ordering

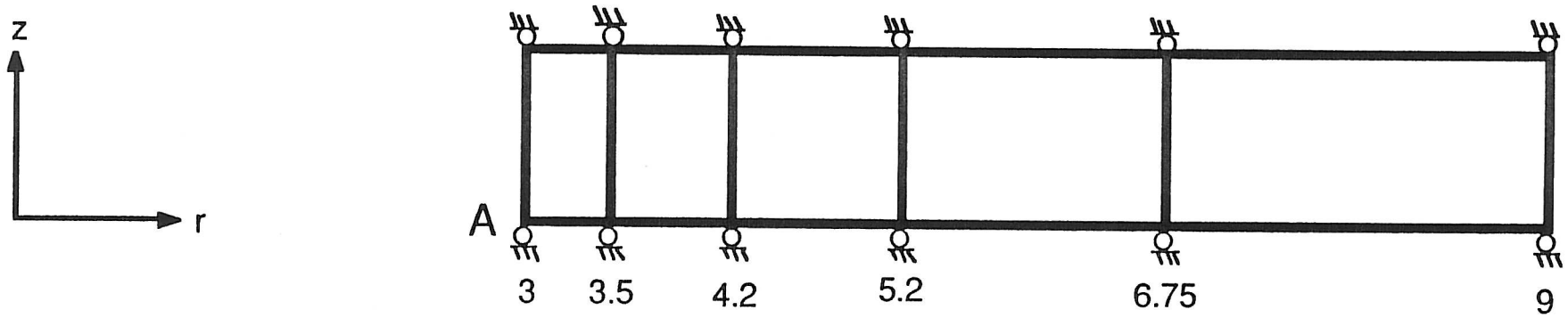

Figure 3.1a. Thick-cylinder, regular mesh

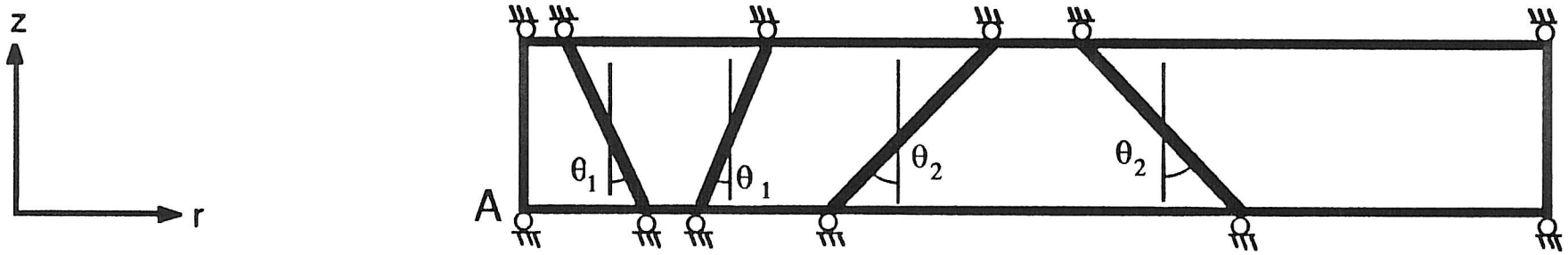

Figure 3.1b. Thick-cylinder, skewed mesh

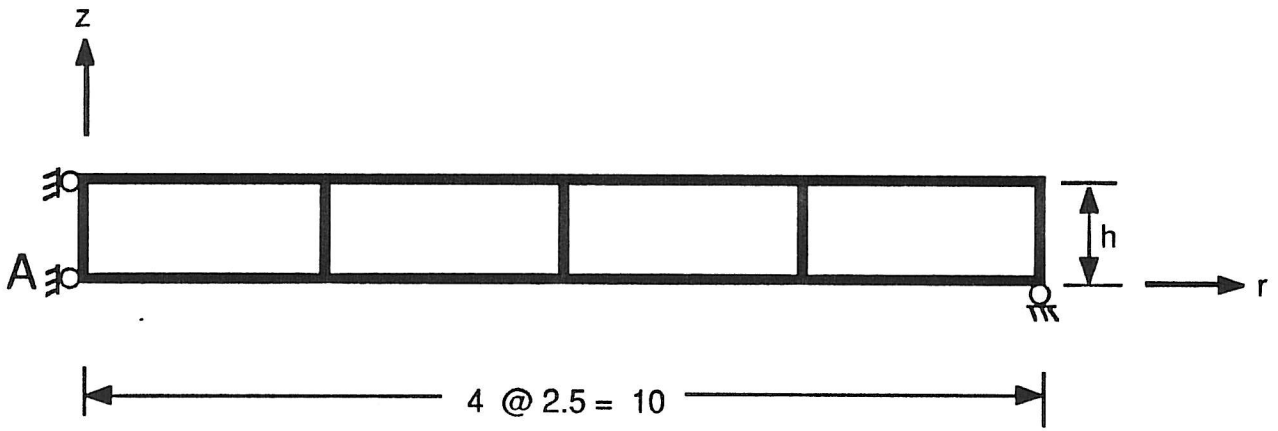

Figure 3.2a. Circular plate, regular mesh

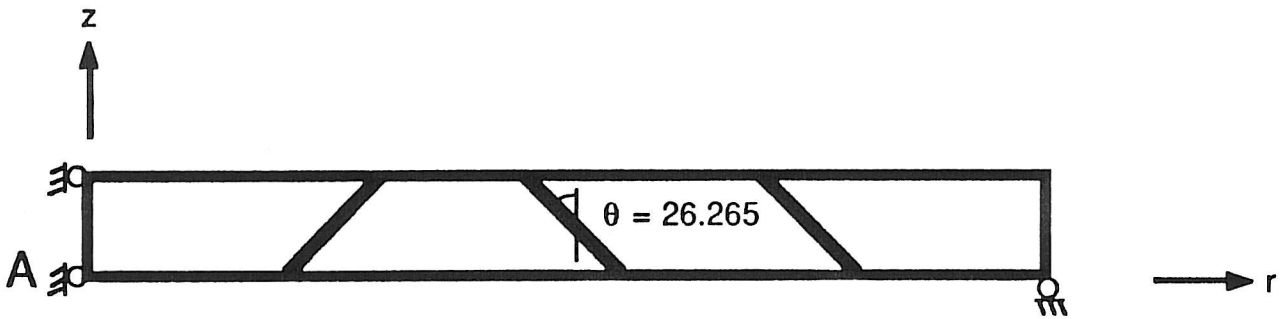

Figure 3.2b. Circular plate, skewed mesh

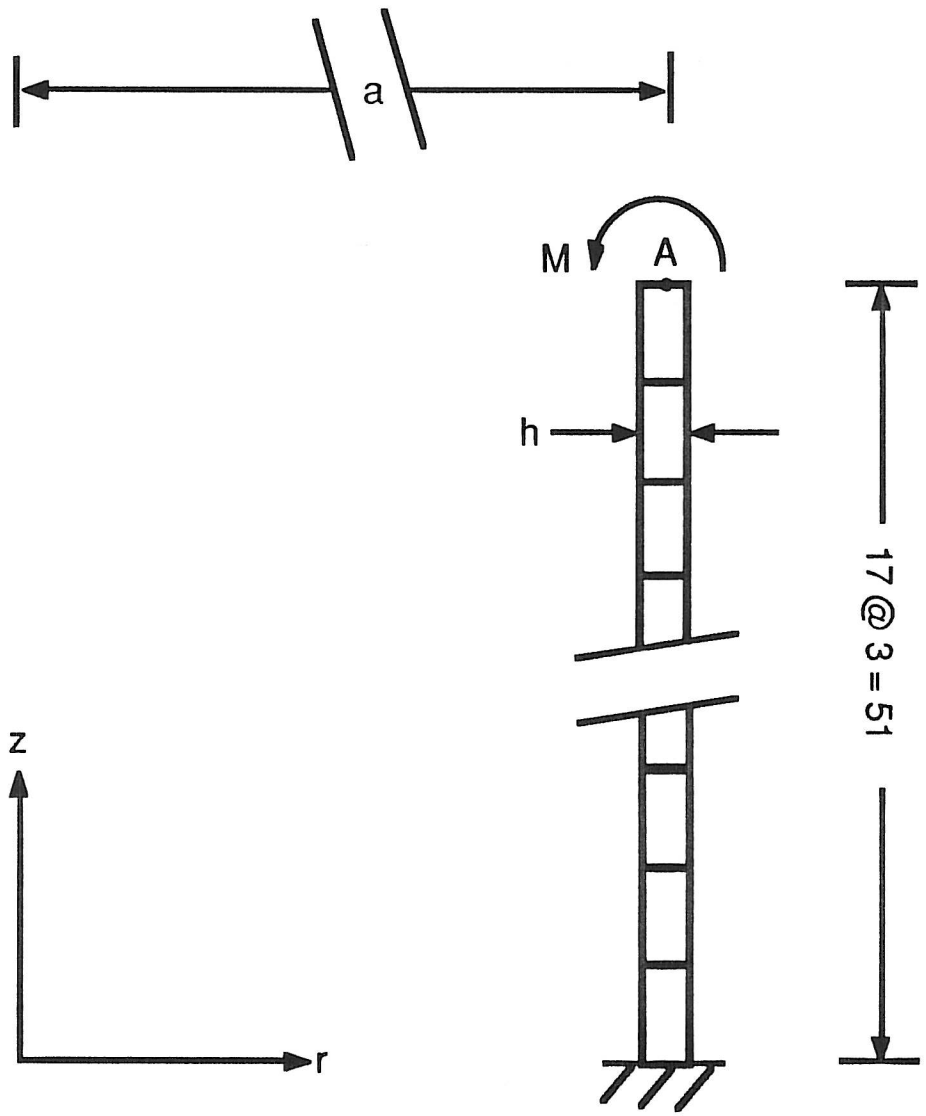

Figure 3.3 Cylinderical shell loaded by an edge moment

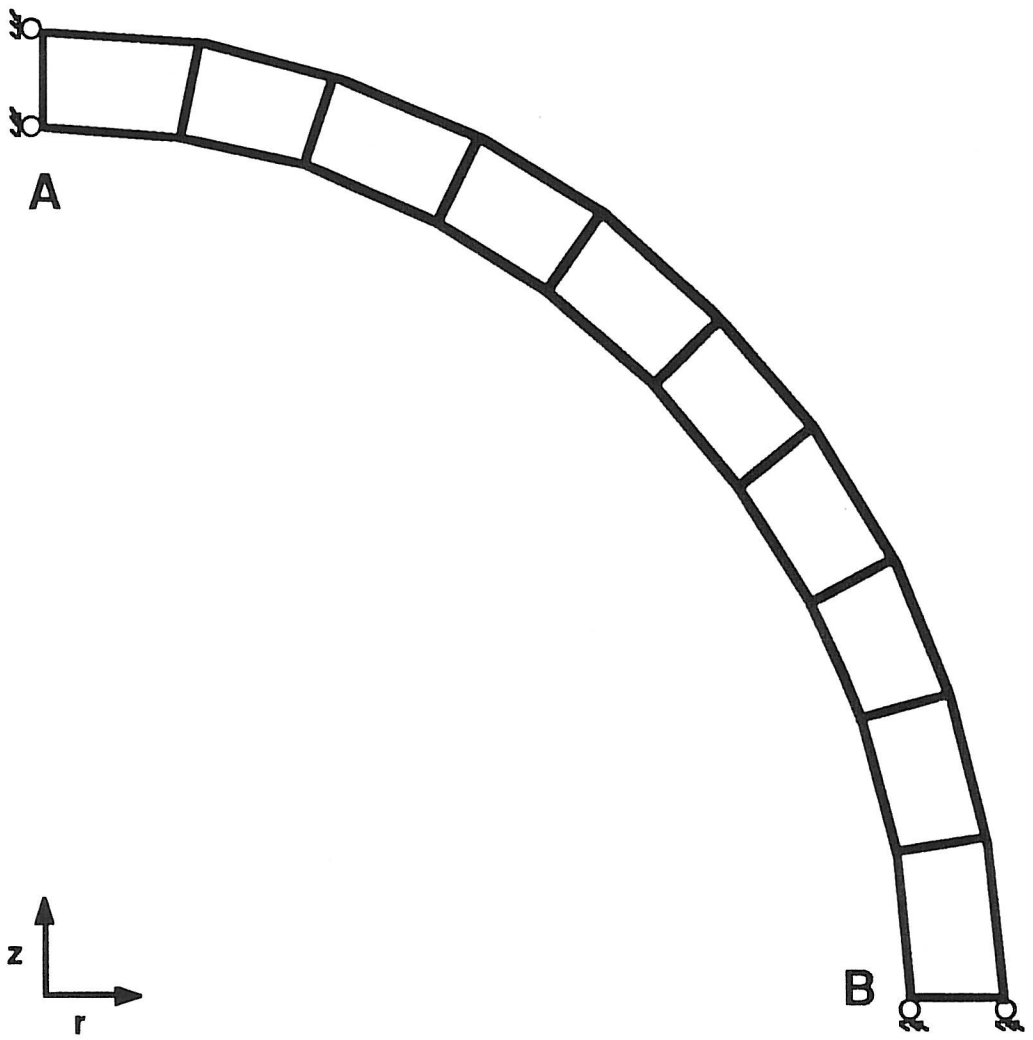

Figure 3.4a. Thin-sphere mesh

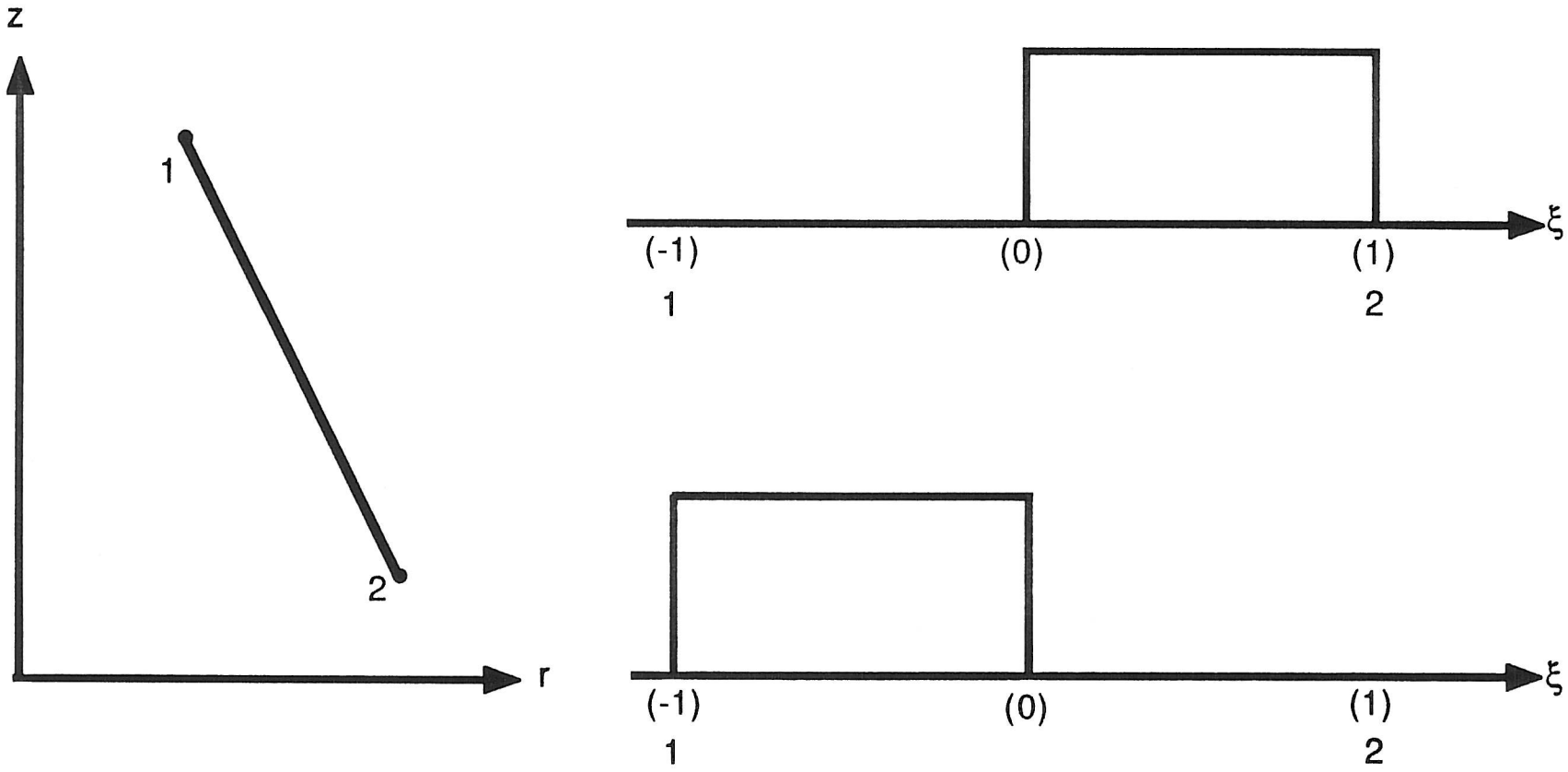

Figure 3.4b. Halleux's shape functions for computing the nodal loads for an axisymmetric shell.

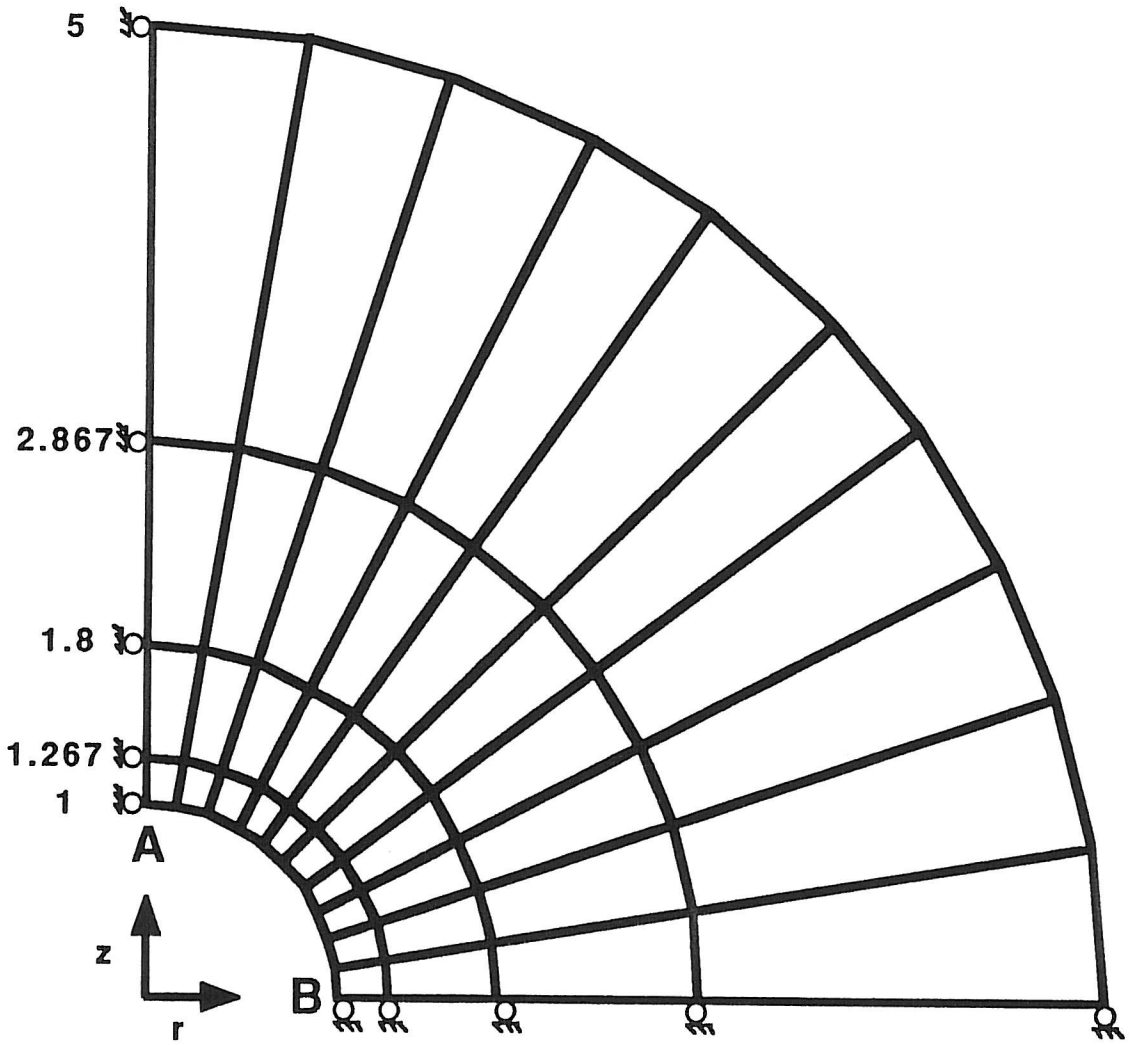

Figure 3.5. Thick-sphere mesh